Electron Flow Modulation in Double-Gap Cavity With a Multiple Ratio of the Two Modes Frequencies

V. Yu Muchkaev, *Member, IEEE*, V. A. Senchurov, S. Kurkin, and A. Badarin

***Abstract*—The study presents the calculation and optimization of the double-gap cavity designs for a klystron-type multipath frequency multiplier. This construction allows to achieve a multiplied (equal to two) ratio of the frequency of the highest (3π) mode to the frequency of the main (2π) mode lying in the *Ka*-range. The design was optimized using a nondimensional quality parameter that combines the main electronic and electrodynamic characteristics of resonators. The features of the electron flow bunching when passing through a double-gap cavity in the two-frequency mode are studied using the 3-D numerical modeling methods. Analysis of the results showed that depending on the ratio of the voltages effective amplitudes generated by electric fields of the main and highest modes, two modulation modes are possible. They are nonsinusoidal modulation, which allows increasing the efficiency at the input signal frequency, and frequency multiplication regime, in which the frequency of the electron flow bunches at the output of the resonator doubles.**

***Index Terms*—Double-gap cavity, klystron frequency multiplier, millimeter (mm) wavelength range, PIC modeling.**

I. Introduction

THE millimeter (mm) and submillimeter (sub-mm) wavelength ranges occupy the spectral region between the microwave and infrared ranges and remain the least developed at the moment. For methods of classical vacuum electronics, these ranges are too short wave, and for methods of quantum electronics, they are too low frequency, resulting in a so-called "terahertz dip" [1], [2].

Significant interest in mm and sub-mm radiation arises from a number of specific features that make it very attractive for a wide range of fundamental and applied research in physics, chemistry, biology, and medicine [3]. Electromagnetic waves of the mm and sub-mm ranges are promising for diagnostics and spectroscopy of various media [4], for creating dense plasma and controlling its parameters [5], in security systems for detecting and identifying objects, in high-resolution medical imaging [6], for creating information transmission systems with ultrahigh bandwidth (up to 10 Gbit/s or more) [7], [8].

Most of these applications require the use of powerful (from several dozens to several thousand watts or more), compact, inexpensive, user-friendly sources [9], which makes researchers look for ways to promote classical vacuum microwave devices (klystrons, TWT, and BWT) in the mm and sub-mm ranges.

Classical methods for increasing the frequency of these devices by reducing the characteristic linear dimensions in the vast majority of cases are difficult to implement due to physical and technological limitations.

Another method is to develop frequency multipliers based on klystron-type devices [10]–[13], TWT [14], and gyrotrons [15]–[17].

This study presents the research results for improving the efficiency of klystron multipliers (KMs). Typically, a KM resonant system consists of input and intermediate single-gap resonators, whose natural frequency is equal to the frequency of the input signal f_{in}, and an output resonator tuned to a multiplied frequency nf_{in} and excited by electron bunches. In turn, their repetition frequency is f_{in}. In such devices, the efficiency may reach up to several percents [13].

Recently, there have been attempts to increase the efficiency of KM by using odd-shaped resonators [11] and working on highest modes [10]. However, the basic concept remains unchanged: the input part of the resonant system has a frequency f_{in} and the output part of the resonant system has a frequency nf_{in}.

This article considers the possibility of increasing the efficiency of KM by using multiband resonators where the frequencies of the two modes have a multiple ratio. The selection of the resonator size can be adjusted so that the frequency of one mode f_0 (from this point on it will be called the main operating mode) is equal to the input frequency f_{in}. At the same time, the frequency of the second mode (indicated as the highest operating mode) is capable of relatively effective

Manuscript received October 8, 2020; revised November 30, 2020; accepted December 16, 2020. The reported study was funded by the Russian Foundation for Basic Research (RFBR) according to the research project No 18-32-20135. The review of this article was arranged by Editor J. Feng. *(Corresponding author: V. Yu Muchkaev.)*

V. Yu Muchkaev and V. A. Senchurov are with the Department of Electronic Devices and Equipment, Yuri Gagarin State Technical University of Saratov, 410054 Saratov, Russia (e-mail: muchkaev_vadim@mail.ru).

S. Kurkin and A. Badarin are with the Neuroscience and Cognitive Technology Lab, Center for Technologies in Robotics and Mechatronics Components, Innopolis University, 420500 Innopolis, Russia.

Color versions of one or more figures in this article are available at https://doi.org/10.1109/TED.2020.3046994.

Digital Object Identifier 10.1109/TED.2020.3046994

This article has been accepted for inclusion in a future issue of this journal. Content is final as presented, with the exception of pagination.

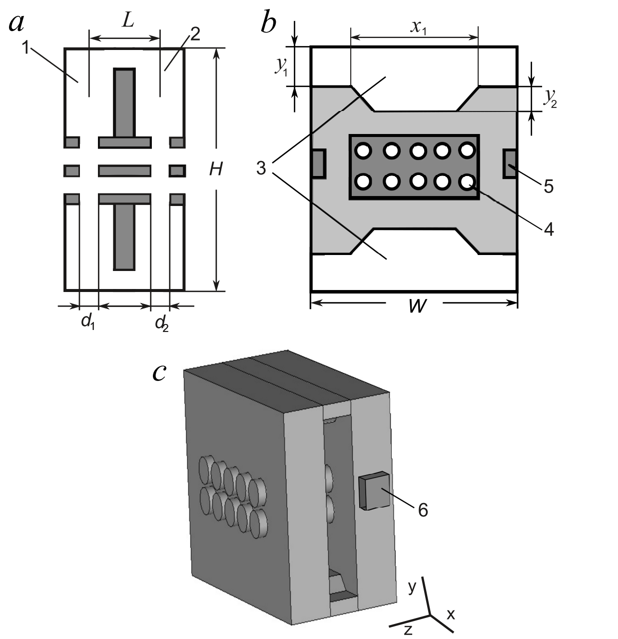

Fig. 1. Schematic of the considered resonator: (a) Longitudinal section of the double-gap cavity. (b) Cross section. (c) Vacuum part of the double-gap cavity.

interaction with an electron flow equals to $f_n = nf_0$, where n is the order of multiplicity [18]. If the electron flow excites high operating mode while passing the resonator, the mutual action of the basic and highest operating modes may lead to the emergence of electron bunches with a repetition rate of nf_{in} [19].

II. Design of the Studied Resonator

The design of the double-gap cavity is shown in Fig. 1. It is formed by resonant chambers 1 and 2 with the shape of a block and are separated by an H-shaped wall (see Fig. 1). Thus, the connection between the neighboring resonant chambers was carried out using two T-shaped communication slits 3. Ten cylindrical channels 4 of radius $\boldsymbol{r_a}$ were placed in the center of the cavity for the passage of a multipath electron flow. Additional elements 5 were provided for fine frequency tuning and control. They are cylindrical rods with a radius of 0.4 mm. The modulating signal was fed through slit 6 in the sidewall of the cavity.

The following was selected as the initial values.

1) The height H and width W of each prismatic chamber were equal to $\lambda_0/2$, where $\lambda_0 = c/f_0$ is the wavelength of the main operating mode with a frequency of f_0 and c is the speed of light in vacuum.
2) All gaps had the same width $d = d_1 = d_2$.
3) The resonator is formed by resonant chambers of the same height $h = h_1 = h_2$.

The resonator dimensions were found based on the frequency adjustment of the main mode $f_0 \approx 30$ GHz, and hence, $\lambda_0 \approx 10$ mm. The accelerating voltage U_0 was chosen to be 6 kV.

The in-phase mode (2π) was chosen as the main operating mode since it has a number of advantages over the antiphase (π) mode; it has a larger interaction impedance and allows operating at a lower accelerating voltage.

Higher order modes ($m\pi$, where $m > 2$), as a rule, are not used as operating since they interact less efficiently with the electron beams. As a result, the main electrodynamic characteristics (characteristic impedance ρ, coupling factor M, and relative electronic conductivity g_e) of these modes have low values and it is extremely problematic to obtain acceptable values of efficiency and output power. Therefore, these modes are usually considered parasitic.

When calculating the distance between the centers of the gaps L, the study took into account its relation to the accelerating voltage, the resonant frequency, the phase shift of the field, and the electron transit angle $\varphi_0 = \omega_0 L/v_0$, where $\omega_0 = 2\pi f_0$, $v_0 = (2eU_0/m_e)^{1/2}$ is the electron velocity at the input of the resonator, and e and m_e are the charge and mass of the electron, respectively. It is known that in buncher resonator with the operating in-phase mode, the transit angle is 2π. Considering the selected values f_0 and U_0, the distance L was 1.71 mm.

The remaining dimensions of the resonators were found by calculating the distribution of the electromagnetic field in the resonator using the finite-difference time-domain (FDTD) method with a rectangular spatiotemporal partition grid in case of three dimensions [20]–[22]. The field in the resonator was excited by a sinusoidal soft source with a Gaussian envelope. The walls of the resonator were taken as the perfect conductor. Since this method works in the time domain, it is best suited to the task of the study since it allows to immediately get a result for a wide range of frequencies in a single calculation.

The adequacy of the software implementation of the FDTD method is verified by solving test tasks with a known solution and comparing the calculation results with experimental data [23].

The analysis of the Fourier spectrum and distributions of the electromagnetic field indicates that in a double-gap cavity, the frequency value of the fifth highest mode (3π) is close to $2f_0$, and the distribution of the longitudinal component of its electric field in the interaction area is fairly uniform. The frequencies of 2π and 3π modes were adjusted by introducing elements 5 into the resonant area, change in the height H, and the parameters of the coupling slits x_1, y_1, and y_2 (see Fig. 1). At the same time, the introduction of adjustment elements 5 and changes in height H had a greater effect on the frequency 2π mode, and the frequency adjustment 3π mode was performed by changing the dimensions x_1, y_1, and y_2.

III. Design Optimization

To optimize the resonator design, the study used a dimensionless quality parameter introduced in [24]

$$T = \frac{\bar{\rho}\bar{M}^2 S}{\eta_0 \lambda^2}. \tag{1}$$

where $\eta_0 = 120\pi\ \Omega$ is the characteristic resistance of free space, $\lambda = c/f$ is the natural wavelength of the operating mode, $S = \pi r_b^2$ is the interaction area, r_b is the radius of one electron beam, $r_b/r_a = 0.6$, $\bar{\rho}$ is the characteristic impedance of the resonator averaged over the interaction area S, and

$\bar{M}$ is the coupling factor of the resonator averaged over the interaction area S. This parameter allows comparing the efficiency of the interaction of the electromagnetic field of the resonator with the electron beam and the maximum beam current at a given current density for resonators designed for different natural frequencies and accelerating voltages.

The average values of the characteristic impedance $\bar{\rho}$ and the coupling factor $\bar{M}$ and the Q-factor were calculated by numerical integration using the formulas [25]–[27]

$$\bar{\rho} = \frac{1}{S}\int_S \rho(x,y)ds = \frac{1}{2\omega_0 WS}\int_S \left(\int_{z_1}^{z_2} |E_z(x,y,z)|dz\right)^2 ds \tag{2}$$

$$\bar{M} = \frac{1}{S}\int_S M(x,y)ds = \frac{1}{S}\int_S \left(\frac{\int_{z_1}^{z_2} E_z(x,y,z)\exp(-j\beta_e z)dz}{\int_{z_1}^{z_2} |E_z(x,y,z)|dz}\right)ds. \tag{3}$$

$$Q = \frac{2\pi f_0 W_r}{P_{\mathrm{v}} + P_S} \tag{4}$$

where $E_z(x,y,z)$ is the distribution function of the longitudinal component of the electric field strength, $W_r = 0.5\int_{\mathrm{v}} \varepsilon_0 E^2 d\mathrm{v}$ is the electromagnetic energy, v is the volume of the studied resonator, $\beta_e = \omega_0/v_0$ is the the propagation constant, $P_{\mathrm{v}} = \pi f_0 \varepsilon_0 \varepsilon_r \tan(\delta)\int_{\mathrm{v}} |E|^2 d\mathrm{v}$ is the dielectric loss, $\varepsilon_0 = 8.85 \times 10^{-12}$ F/m, ε_r is the relative permittivity, $\tan(\delta)$ is the dielectric loss tangent, $P_S = (1/2)((\pi\mu f_0/\sigma))^{1/2}\int_S |H_{\tan}|^2\, ds$ is the surface losses, μ is the magnetic permeability of wall metal, σ is the specific conductivity, and $H_{\tan}$ is the tangential component of magnetic field strength.

The calculated dependences of the quality parameter T on the normalized gap width d/r_a for the in-phase mode and the fifth highest mode at different values of the radius of the transit channel r_a are shown in Fig. 2. The type of these dependences is determined by the change in the characteristic impedance $\bar{\rho}$ and the coupling factor $\bar{M}$: the growth of the $\bar{\rho}$ and the decrease of the $\bar{M}$ with increasing d/r_a.

The in-phase mode frequency was adjusted by inserting tuning rods 5 (see Fig. 1) into the resonant region, and the highest mode frequency was adjusted by changing the parameters y_1 and y_2 (curves 1–3 in Fig. 2). As follows from the obtained results, the best design is one with a radius of transit channels $r_a = 0.25$ mm, which is considered in the future.

In case of the maximum value of T at $d/r_a = 1.2$, the characteristic impedance in the central transit channels in the in-phase mode ρ_{01} was 86.3 Ω, and in the highest mode—$\rho_{h1} = 8.6$ Ω. In the off-center transit channels in the in-phase mode, the characteristic impedance was $\rho_{03} = 57.3$ Ω, at the highest—$\rho_{h3} = 6.9$ Ω.

The results of calculations show that it is possible to reduce the unevenness of the longitudinal distribution of the electric field in the interaction area by reducing the width of the gaps while reducing the size H (see Fig. 1). Fig. 3(a) shows the dependences of the ratios $k_0 = \rho_{01}/\rho_{03}$ (curve 1) and $k_h = \rho_{h1}/\rho_{h3}$ (curve 2) on d/r_a, which decreases linearly as the

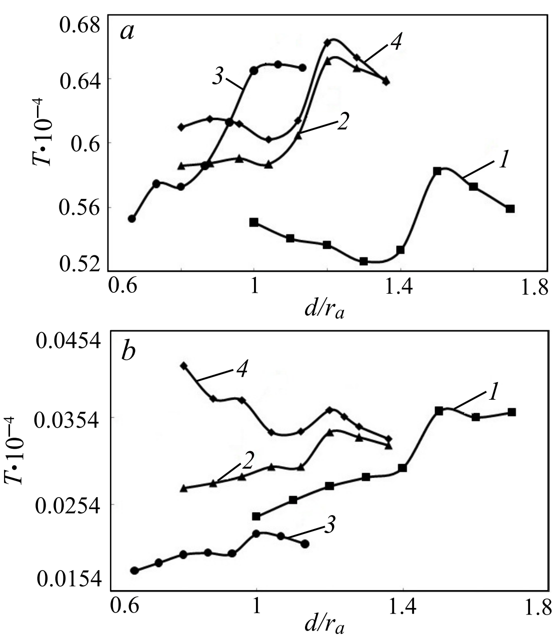

Fig. 2. Dependences of the quality parameter T on the normalized width of gaps d/r_a for (a) 2π and (b) 3π modes at different values of the radius of the transit channels in a double-gap cavity: curves 1 are calculated at $r_a = 0.2$ mm, curves 2 and 4 are calculated at $r_a = 0.25$ mm, and curves 3 are calculated at $r_a = 0.3$ mm. When calculating curves 1–3, the frequency adjustment of the 2π mode was carried out by introducing tuning elements 5 into the resonant region (see Fig. 1), when calculating curves 4—by changing the height H (see Fig. 1).

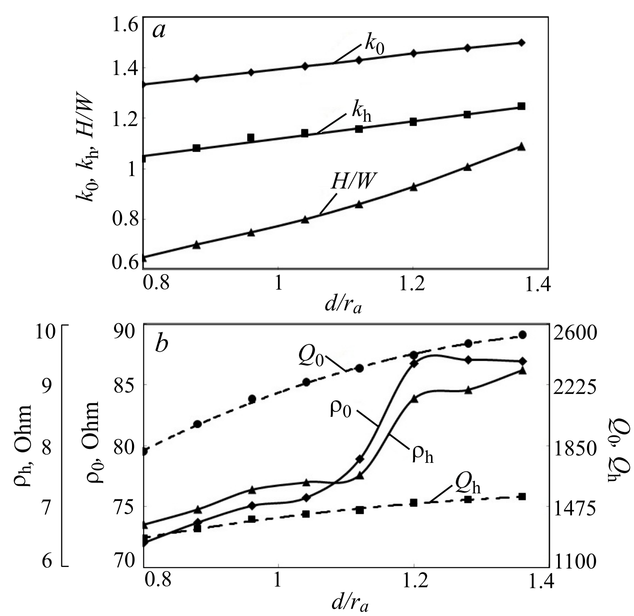

Fig. 3. (a) Calculation results for a double-gap cavity with a transit channel radius $r_a = 0.25$ mm. (b) Dependences of characteristic impedance in-phase ρ_0 and the fifth highest ρ_h modes calculated in the central transit channel.

gap width decreases. Curve 3 shows the relative change in the resonator parameter H due to which the frequency of the in-phase mode was adjusted.

The dependences of the quality parameter T in this case are reflected in curves 4 in Fig. 2(a) and (b). As can be seen

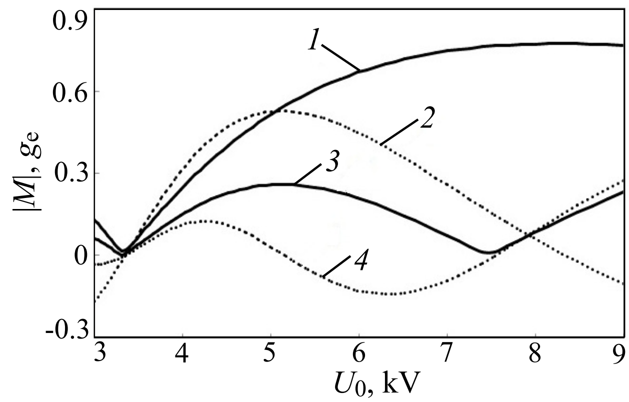

Fig. 4. Dependences of the modulus of the interaction coefficient M (curves 1 and 3) and the relative electronic conductivity g_e (curves 2 and 4) for the double-gap cavity. Curves 1 and 2 are obtained for the 2π mode, and curves 3 and 4 are obtained for the 3π mode.

from the obtained data, when the H/W ratio decreases, the T value increases for both modes. Here, the qualitative form of the dependence of T on d/r_a for the 3π mode changes; with a decrease in the gap width, the value of the quality parameter increases. This is explained by the fact that, in this case, with a decrease in the d/r_a ratio, the resonator frequency was tuned by decreasing the parameter H. The consequence of this is a decrease in the resonator volume, which leads to a decrease in the electromagnetic field energy W_r. Since the relationship between the characteristic impedance and the energy of the electromagnetic field is inversely proportional (2), this partly compensates for the decrease in ρ with a decrease in the d/r_a. As a result, the dependence of the quality parameter T in this case differs from the case when the height H is constant [curves 1–3 in Fig. 2(b)].

Considering that with a decrease in the gap width, the characteristic impedance [curves 1 and 2 in Fig. 3(b)] and the Q-factor [curves 3 and 4 in Fig. 3(b)] of the resonator decreases, the design of a double-gap cavity with the following dimensions was chosen as a compromise option for further research: the radius of the transit channels $r_a = 0.25$ mm, the relative width of the gaps $d/r_a = 0.96$, and the ratio of the sides of the resonator $H/W = 0.75$. In this case, $\rho_{01} = 75.1\ \Omega$, $\rho_{03} = 54.2\ \Omega$, $\rho_{h1} = 7.3\ \Omega$, $\rho_{h3} = 6.5\ \Omega$, $Q_0 = 1395$, and $Q_h = 2135$.

Fig. 4 shows the calculated dependences of the coupling factor M (curves 1 and 2) and the relative electronic conductivity g_e (curves 3 and 4) on the accelerating voltage U_0. The g_e value was calculated by numerical differentiation using the formula given in the paper [28]

$$g_e = -\frac{\beta_e}{4}\frac{\partial|\mathbf{M}|^2}{\partial\beta_e}. \tag{5}$$

The obtained results (curves 2 and 4 in Fig. 4) show that in case of the selected value of the accelerating voltage $U_0 =$ 6 kV and the transit angle between the gaps equal to 2π, the value of the relative electronic conductivity is positive for 2π and negative for 3π.

IV. Bunching of the Electron Flow When Passing Through the Double-Frequency Double-Gap Resonator

Let us consider the conditions for the excitation of the highest operating mode with a frequency of $2f_0$ in the studied double-gap cavity and the effect of this mode field on the bunching of the electron flow.

To solve this problem, a mathematical model based on solving a self-consistent system of Maxwell–Vlasov equations in the 2-D case has been developed. In this case, the electromagnetic fields are calculated directly by solving Maxwell's equations using the finite-difference method with boundary conditions corresponding to ideally conducting walls of the interaction space. The Maxwell equations are solved in a rectangular coordinate system on spatiotemporal grids with constant time steps. The electron flow moving in the transit channels is represented by a flow of "macroparticles" with the same specific charge equal to the electron charge [29], [30]. Integral characteristics (charge density, current density, and so on) are found by weighing particles on a spatiotemporal grid and then used to find electromagnetic fields in the calculated area.

In the simulation, the magnetic field had only a longitudinal component $B_z = 0.25$ T. The signal at frequency f_0 was fed into the first resonant chamber through a rectangular slit 6 (see Fig. 1) in the sidewall of the resonator with height H. The location and dimensions of the slit were selected to minimally load the highest mode with a multiplied frequency and at the same time to provide an optimal load on the in-phase mode. The input power varied from 1.5 to 4 W.

The calculated electrodynamic and electronic parameters (characteristic impedance, coupling factor, relative electronic conductivity, and Q-factor) of the resonator for the considered modes allowed to estimate the minimum current at which the highest mode can be excited with a frequency of $2f_0$ from the amplitude condition of self-excitation [31]. In case of a double-gap cavity, the expression for calculating the value of the minimum starting current on the mth mode can be written as follows:

$$I_s = \frac{2U_0}{\rho_m Q_m g_{2em}}. \tag{6}$$

where ρ_m, Q_m, and g_{2em} are the characteristic impedance, unloaded Q-factor, and relative electronic conductivity of the second resonator gap on the mth mode, respectively.

Since the characteristic impedance averaged over the gaps at 3π mode was about 7 Ω, the unloaded Q-factor $Q_h = 2135$, and the relative electronic conductivity of the second gap $g_{2eh} = 0.105$, the minimum starting current was 7.6 A at the selected accelerating voltage of 6 kV.

The density of commonly used thermocathodes does not exceed 20 A/cm^2, so the maximum current of the electron flow I_0 will be 0.141 A. Thus, at this current value, 3π, mode should not be excited. This follows from the analysis of the Fourier spectrum of the electromagnetic field oscillations inside the resonator when the frequency of the highest

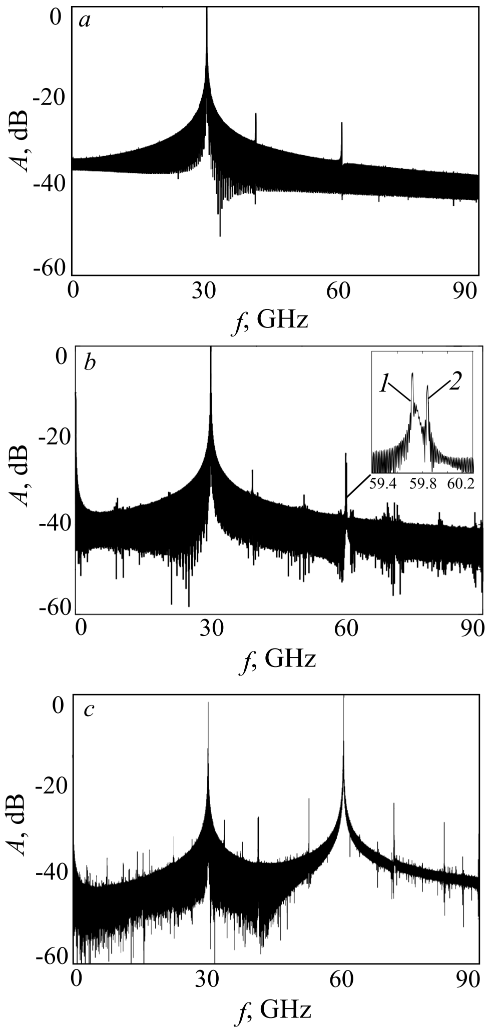

Fig. 5. Fourier spectra of electromagnetic field oscillations inside a double-gap cavity in steady-state regime when an input signal is applied with a frequency $f_{\text{in}} = 29.92$ GHz. (a) Detuning $\delta_f = |2f_{\text{in}} - f_h| > 500$ MHz. (b) $\delta_f \approx 200$–300 MHz. (c) $\delta_f \approx 0$.

operating mode f_h is not equal to twofold frequency of the input signal f_{in} [see Fig. 5(a)]. In this case, there are basically two components in the spectrum. The main component has the frequency f_{in} and the harmonic component with the frequency $2f_{\text{in}}$, the amplitude of which depends on a number of factors: the power of the input signal P_{in}, the difference between f_{in} and f_0, and so on.

When the value of the f_h/f_{in} ratio approaches 2, in addition to the frequencies of the input signal and the second-harmonic component [number 1 in Fig. 5(b)], another component with the frequency f_h [number 2 in Fig. 5(b)] emerges in the spectrum of the electromagnetic field oscillations inside the resonator. The detuning $\delta_f = |2f_{\text{in}} - f_h|$, where f_h can be observed, is determined mainly by the power of the input signal and the value of the loaded Q-factor at the highest mode. δ_f was usually 200–300 MHz.

With the onset of resonance (i.e., when $\delta_f \approx 0$), the amplitude of the highest mode begins to increase and, in the steady state, may exceed the amplitude of the main mode [see Fig. 5(c)]. In this case, the oscillation frequency is $2f_{\text{in}}$, that is, the frequency of the highest mode f_h is captured.

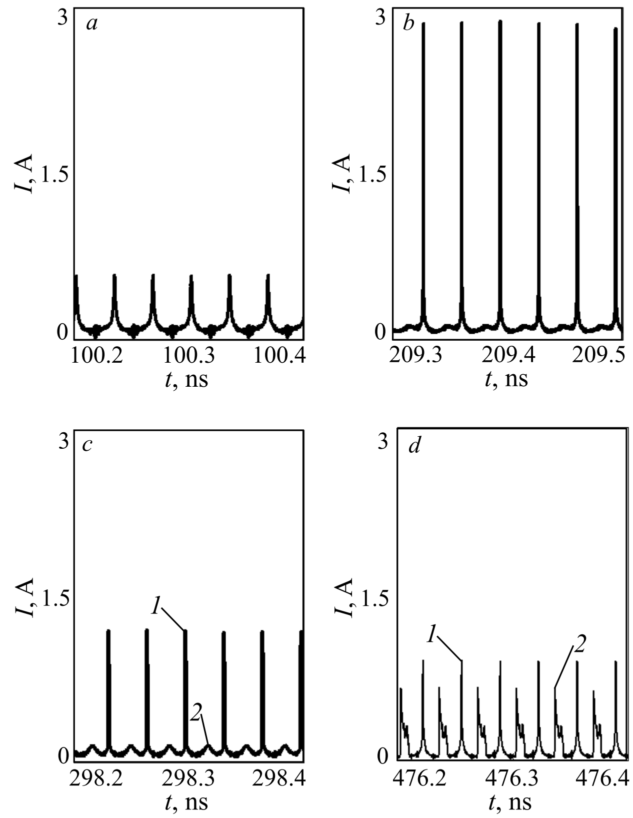

Fig. 6. Change in time of the electron flow current passing through the plane located at a distance from the center of the second gap of the double-gap cavity, corresponding to the transit angle 4π. Input signal frequency $f_{\text{in}} = 29.92$ GHz, power $P_{\text{in}} = 3.6$ W, and electron flow current $I_0 = 0.14$ A. Number 1 indicates electron bunches following the frequency f_{in}, and number 2 indicates electron bunches formed under the action of the field 3π mode.

In this regime, as the amplitude of the electromagnetic field oscillations increases at the frequency $2f_{\text{in}}$, the appearance of the electron flow bunches that passed through the resonator significantly changes. At the beginning of the transition period, when the amplitude of the highest mode is still small, the type of electron current bunches does not differ from the case of $f_h/f_{\text{in}} \neq 2$ [see Fig. 6(a)].

As the amplitude of the highest mode increases, the amplitude of the current bunches also increases [see Fig. 6(b)], and the bunches become more dense. The increase in the quality of modulation is explained by the fact that the total effect of the fields of the main and highest modes approaches the sawtooth waveform, which is known to be the most optimal [32]. This regime (let us call it regime A) can be used to achieve the maximum efficiency values in klystron-type amplifiers. It is possible to limit the further growth of the 3π mode amplitude at the value that provides this regime by selecting the necessary value of the loaded Q-factor.

It is worth noting that the designs of resonators with a multiple frequency ratio of the two fundamental modes, which were supposed to be used to improve the bunching of the electron flow, were proposed earlier [33]. However, to implement a double-frequency modulation mode in the resonator proposed in [33], the input signal should also be two-frequency: with the main f_{in} and a multiple $2f_{\text{in}}$ spectral components.

Here, the input signal has only one spectral component with the frequency f_{in}.

Further growth of the field amplitude of the highest mode leads to a decrease of the amplitude of the bunches of current electron flow at a frequency of main signal [designated 1 in Fig. 6(b)], and the appearance of bunches formed field of highest mode [designated 2 Fig. 6(c)]. The amplitude of the latter, as the energy of the 3π type increases, increases too and, in the steady-state mode, can be compared with the amplitude of the bunch formed by the signal of the main frequency f_{in} [designated 2 at Fig. 6(d)]. This regime (let us call it regime B) should be used in klystron-type frequency multipliers.

The output time t_A to regime A decreases with increasing input signal power: $t_A = 420$ ns at $P_{\mathrm{in}} = 1.6$ W and $t_A = 200$ ns at $P_{\mathrm{in}} = 3.6$ W.

The transition time t_{AB} between regimes A and B has an inverse relationship: with increasing input signal power it increases: $t_{\mathrm{AB}} = 180$ ns for $P_{\mathrm{in}} = 1.6$ W and $t_{\mathrm{AB}} = 260$ ns for $P_{\mathrm{in}} = 3.6$ W.

V. Conclusion

The analysis of the results shows that in the double-gap cavity in case of a multiple frequency ratio of the highest (3π) and main (2π) modes equal to 2, the highest mode can be excited even if the electron flow current is lower than the minimum current required for self-excitation. The excitation of the highest mode occurs due to the pumping of energy from the electron flow, which oscillates with the frequency of the input signal f_{in} to the electromagnetic field of the highest mode.

As the amplitude of the highest mode increases, its influence on the modulation of the electron flow increases, and the total HF voltage at the resonator gaps approaches the sawtooth waveform. This leads to improved modulation of the electronic flow at the frequency of the input signal f_{in} (regime A).

A further increase in the amplitude of the field of the highest mode leads to a doubling of the frequency of electron bunches at the output of the resonator (regime B).

References

[1] V. L. Bratman, A. G. Litvak, and E. V. Suvorov, “Mastering the terahertz domain: Sources and applications,” *Phys.-Uspekhi*, vol. 54, no. 8, pp. 837–844, Aug. 2011.

[2] A. D. Grigoriev, “Terahertz electronics,” in *Proc. Int. Conf. Actual Problems Electron Devices Eng. (APEDE)*, Saratov, Russia, 2018, pp. 5–10.

[3] M. Tonouchi, “Cutting-edge terahertz technology,” *Nature Photon.*, vol. 1, no. 2, pp. 97–105, Feb. 2007, doi: 10.1038/nphoton.2007.3.

[4] J. F. Federici, R. L. Wample, D. Rodriguez, and S. Mukherjee, “Application of terahertz Gouy phase shift from curved surfaces for estimation of crop yield,” *Appl. Opt.*, vol. 48, no. 7, pp. 1382–1388, Aug. 2009. [Online]. Available: https://doi.org/10.1364/AO.48.001382

[5] V. M. Isaev, I. N. Kabanov, V. V. Komarov, and V. P. Meshchanov, “Modern radio-electronic systems of terahertz frequency range,” *Proc. TUSUR Univ.*, vol. 34, no. 4, pp. 5–21, Dec. 2014.

[6] Z. D. Taylor *et al.*, “ETHz medical imaging: *In vivo* hydration sensing,” *IEEE Trans. THz Sci. Technol.*, vol. 1, no. 1, pp. 201–219, Sep. 2011, doi: 10.1109/TTHZ.2011.2159551.

[7] A. D. Grigoriev, “Problems in the development of sources of powerful coherent terahertz radiation,” in *Proc. All-Russian Conf. Electron. Microelectron. Microw.*, Petersburg, Russia, 2015, pp. 139–143.

[8] V. Vishnevskyi, S. Frolov, and I. Shakhnovitch, “Radio relay millimeter wave communication systems: New velocity horizons,” *Electron. STB*, vol. 107, no. 1, pp. 90–97, 2011.

[9] J. Federici and L. Moeller, “Review of terahertz and subterahertz wireless communications,” *J. Appl. Phys.*, vol. 107, no. 11, Jun. 2010, Art. no. 111101, doi: 10.1063/1.3386413.

[10] G. Burt *et al.*, “A millimeter-wave klystron upconverter with a higher order mode output cavity,” *IEEE Trans. Electron Devices*, vol. 64, no. 9, pp. 3857–3862, Sep. 2017.

[11] F. Toufexis *et al.*, “Experimental demonstration of a 5th harmonic mm-wave frequency multiplying vacuum tube,” *Appl. Phys. Lett.*, vol. 110, no. 26, Jun. 2017, Art. no. 263507, doi: 10.1063/1.4990970.

[12] B. B. van Iperen and H. Tjassens, “An experimental CW klystron for generating 0.4-mm waves,” *IEEE Trans. Electron Devices*, vol. ED-17, no. 4, pp. 380–382, Apr. 1970.

[13] J. Fan and Y. Wang, “A 14 kW high-power X-band to ka-band klystron frequency multiplier,” *IEEE Trans. Electron Devices*, vol. 61, no. 6, pp. 1854–1858, Jun. 2014.

[14] K. V. Belov, T. A. Karetnikova, A. E. Ploskikh, N. M. Ryskin, and G. V. Torgashov, “Multiplier for 0.2 THz with a sheet electron beam,” *Radio Eng.*, vol. 7, pp. 19–23, Jul. 2017.

[15] I. V. Bandurkin and A. V. Savilov, “Suppressing electron bunching at low harmonics in gyromultipliers of the klystron type,” *Tech. Phys. Lett.*, vol. 33, no. 9, pp. 795–798, Sep. 2007.

[16] I. V. Bandurkin, V. L. Bratman, A. V. Savilov, S. V. Samsonov, and A. B. Volkov, “Experimental study of a fourth-harmonic gyromultiplier,” *Phys. Plasmas*, vol. 16, no. 7, Jul. 2009, Art. no. 070701.

[17] V. L. Bratman, Y. K. Kalynov, and V. N. Manuilov, “Large-orbit gyrotron operation in the terahertz frequency range,” *Phys. Rev. Lett.*, vol. 102, no. 24, Jun. 2009, Art. no. 245101.

[18] V. Y. Muchkaev and V. A. Senshurov, “Electrodynamic characteristics of multiple beam millimeter wave double-gap resonators,” *Radio Eng.*, vol. 2, pp. 99–103, Feb. 2017.

[19] V. Muchkaev, A. Onishchenko, V. Tsarev, and V. Senchurov, “Double-gap multiple-beam resonator with a higher order mode,” in *Proc. Int. Conf. Actual Problems Electron Devices Eng. (APEDE)*, Saratov, Russia, Sep. 2020, pp. 56–58.

[20] S. M. Dennis, *Electromagnetic Simulation Using the FDTD Method*. New York, NY, USA: IEEE Press, 2000, pp. 79–88.

[21] J.-P. Berenger, “A perfectly matched layer for the absorption of electromagnetic waves,” *J. Comput. Phys.*, vol. 114, no. 2, pp. 185–200, Oct. 1994.

[22] K. S. Kunz and R. J. Luebbers, *The Finite Difference Time Domain Method for Electromagnetics*. New York, NY, USA: CRC Press, 1993, pp. 29–48.

[23] V. A. Tsarev, V. Y. Muchkaev, and P. D. Shalaev, “Studying a multibeam microwave drift-tube K-band oscillator with an electrodynamic system of two slot-coupled resonators,” *Tech. Phys. Lett.*, vol. 40, no. 4, pp. 288–292, Apr. 2014.

[24] A. D. Grigoriev, G. Ol’khovik, and S. A. Silaev, “Comparative analysis of resonators O-type devices with spatially developed electron beams,” *Electron. Technics. Microw. Electron.*, vol. 383, no. 11, pp. 9–12, 1985.

[25] A. D. Grigoryev and V. B. Yankevich, *Resonators Resonator Microwave Deceleration Systems Numerical Calculation Design Methods*. Moskow, Russia: Radio and Communication, 1984, pp. 14–21.

[26] M. M. Carliner, *Electrodynamics Microwave: The Course Lectures*. Novosibirsk, Russia: Novosibirsk State Univ., 2006, pp. 202–206.

[27] V. A. Tsarev and V. Y. Muchkaev, “3-D evaluation of energy extraction in multitube double-gap resonator installed downstream of a multibeam klystron,” *IEEE Trans. Plasma Sci.*, vol. 47, no. 1, pp. 214–218, Jan. 2019.

[28] G. Caryotakis, “High power klystrons: Theory and practice at the stanford linear accelerator center,” Stanford Linear Accelerator Center, Menlo Park, CA, USA, Tech. Rep. SLAC-PUB, 2005. Accessed: Jan. 2005. [Online]. Available: https://www-spires.slac.stanford.edu/cgi-wrap/getdoc/slac-pub-10620.pdf

[29] A. S. Roshal, *Modeling of Charged Beams*. Moscow, Russia: Atomizdat, 1979, pp. 147–173.

[30] C. Badsel and A. Lengdon, *Plasma Physics and Numerical Simulation*. Moscow, Russia: Energoatomizdat, 1989, pp. 341–366.

[31] V. Y. Muchkaev, V. K. Fedyaev, and V. A. Tsarev, “Numerical investigation of the electrodynamic properties of a K-band multibeam monotron with a three-gap cavity,” *J. Commun. Technol. Electron.*, vol. 61, no. 9, pp. 1034–1038, Sep. 2016.

[32] I. V. Lebedev, *Tekhnika i Pribory SVCH*, vol. 2. Moskow, Russia: Higher School, 1972, pp. 66–69.

[33] S. O. Schriber and D. A. Swenson, “A single-cavity double-frequency buncher,” *IEEE Trans. Nucl. Sci.*, vol. NS-26, no. 3, pp. 3705–3707, Jun. 1979.